Meteorol. Z. (Contrib. Atm. Sci.)
Published online December 2024

Open Access
Early Access Boundary Layer Meteorology

Mesoscale simulations of coastal boundary-layer transitions. Part 1: low-level jets

Mares Barekzai[1,*], Beatriz Cañadillas[2], Stefan Emeis[1], Martin Dörenkämper[3], Astrid Lampert[2]

[1] Institute of Meteorology and Climate Research – Atmospheric Environmental Research (IMK-IFU), Karlsruhe Institute of Technology (KIT), Garmisch-Partenkirchen, Germany
[2] Institute of Flight Guidance, TU Braunschweig, Braunschweig, Germany
[3] Fraunhofer Institute for Wind Energy Systems, Oldenburg, Germany
* Corresponding author: mares.barekzai@posteo.de

With 15 figures and 1 table

Abstract: The impact of coastal low-level jets (LLJs) should be taken into account in the planning and operating phases of offshore wind farms as these elevated wind maxima introduce additional kinetic energy and vertical wind shear at operational heights of typical offshore wind turbines. In this study, the spatial distribution of LLJs in the German Bight was investigated using a twelve-year high-resolution data set computed with the Weather Research and Forecasting Model (WRF). The data set was divided into sectors of different wind directions, and the sectors with offshore oriented wind directions, i.e., wind blowing from land towards the open sea, are analyzed separately. The results show that the occurrence of LLJs strongly depends on wind direction. In general, offshore wind directions have higher probabilities of LLJ occurrence, with a systematically reduced LLJ probability immediately behind the coastline and the highest probability approximately 100–150 km offshore. On average, the probability of LLJ occurrence is highest around a height of 200 m in the vertical profile. The probability distribution of the strength of the LLJ wind speed follows the pattern of the LLJ probability, but the LLJ is less pronounced over water than over land. The seasonal changes in LLJ probability are driven by atmospheric stability, with larger probabilities in spring and summer and smaller probabilities in autumn and winter. On average, the highest LLJ probabilities occur in spring and summer during daytime and the lowest in autumn and winter during nighttime.

Keywords: low-level jet; WRF; German Bight; wind energy; offshore wind farms; SDG7

1 Introduction

The phenomenon of the low-level jet (LLJ) is defined as a maximum wind speed in the atmospheric boundary layer with lower wind speed above it (Baas et al. 2009). LLJs have been studied for decades (Blackadar 1957). When stable atmospheric conditions emerge, and a surface-based temperature inversion occurs, the layers above the inversion become decoupled from the surface friction and are subject to inertial oscillations, resulting in a sudden increase in wind speed for a certain altitude interval. The flow in the residual layer accelerates to super-geostrophic magnitudes, forming a LLJ (Blackadar 1957). The classical conceptual description for LLJs over land is based on an inertial oscillation occurring in the time domain (time elapsed since sunset). LLJs forming with offshore wind direction over the sea are an analogue in the space domain depending on the distance from the coastline, where temperature inversions are formed mainly by advection of warmer air masses (Schulz-Stellenfleth et al. 2022). Both phenomena can be seen as inertial oscillation. Super-geostrophic wind speeds are more likely for onshore LLJs, because onshore surface friction reduces to nearly zero with the formation of a stable surface layer at sunset, while some low surface friction remains even after crossing the coastline.

There are various other causes that can lead to the formation of a low-level jet, including the passage of frontal systems (Doyle & Warner 1993) and katabatic wind systems (Heinemann & Zentek 2021). However, the focus of this article is on the classical development of LLJs, which is related to changes in the atmospheric stratification from turbulently mixed to stably stratified, as described above. Such temperature inversions typically occur during the evening transition on cloudless days above land, when the surface cools down

DOI: 10.1127/metz/2024/1195
Gebrüder Borntraeger Science Publishers, Stuttgart, www.borntraeger-cramer.com

quickly after sunset (Davies 2000). The temperature inversion often intensifies and rises to higher altitudes during the night (Surridge 1986).

On a yearly average, LLJ phenomena occur on 13–52% of all nights in Europe, depending on the location and the applied criteria for identification (Baas et al. 2009; Emeis 2014; Lampert et al. 2015; Marke et al. 2018). The frequency of LLJ events is most significant in summer because onshore LLJ events are related to strong nocturnal temperature inversions induced by surface cooling (Lampert et al. 2015). The statistics of LLJs are expected to vary with climate change (Gross 2012).

LLJ statistics based on ERA-Interim reanalyses data reveal a frequent occurrence of strong LLJs at the western coast of the continents (Ranjha et al. 2013) and in coastal areas (Tuononen et al. 2015). Both of these studies do not identify the coast of the North Sea as an area of particular LLJ activity, but they apply the strict criteria of 2 m/s and 25% wind speed reduction from the core to the minimum above, which exclude the identification of less pronounced LLJ events.

The maximum altitude of the LLJ is often located below the top of the temperature inversion (Andreas et al. 2000; Tjernström et al. 2004; Wagner et al. 2019). Coastal areas typically have a maximum wind speed altitude below 200 m (Kalverla et al. 2019), within the altitude range of offshore wind turbine rotor blades. Therefore, understanding the LLJ phenomenon recently gained worldwide importance, especially with the increasing hub heights and rotor diameters of wind turbines. Wind energy already plays a significant role in current and future worldwide energy supply (Veers et al. 2019). LLJs can increase wind power production, particularly in the wind speed range below the rated speed (Wagner et al. 2009). However, LLJ events are associated with enhanced wind shear, which is typically in the height range of the rotor blades (Wagner et al. 2011, 2014). LLJs have positive and negative shear regions in their velocity profile. The positive shear regions are continuously turbulent, while the negative shear regions have limited turbulence (Gadde & Stevens 2021).

In wind farms, large eddy simulations (LES) show that when the LLJ wind speed maximum is above the turbines, wake recovery is relatively fast (Gadde & Stevens 2021). This is due to the high turbulence below the LLJ and the downward vertical entrainment created by the momentum deficit due to the wind farm's conversion of kinetic to electric energy (Gadde & Stevens 2021). In contrast, when the LLJ is below the turbine rotor swept area, the wake recovery is very slow due to the low atmospheric turbulence above the LLJ. The energy budget analysis reveals that the entrainment fluxes are maximum and minimum when the LLJ wind speed maximum is above and in the middle of the turbine rotor swept area, respectively. Surprisingly, the negative shear creates a significant entrainment flux upward when the LLJ maximum wind speed is below the turbine rotor swept area, facilitating energy extraction from the jet, which is beneficial for the performance of downwind turbines (Gadde & Stevens 2021). Additionally, this enhanced shear is a source of atmospheric turbulence, leading to increased stress and changes in vibrations, and finally fatigue loadings of rotor blades (Gutierrez et al. 2016), thus reducing the lifetime of wind turbine structures.

Understanding wind speed profiles that deviate from the standard reference logarithmic profile (IEC 2022) is crucial not only for the current extraction of wind energy using conventional wind turbines, but also for new methods, such as floating platforms (Manzano-Agugliaro et al. 2020) and tethered kite systems with flexible altitude of operation (Perkovic et al. 2013). The frequency and intensity of LLJs may have implications for the design and operation of wind energy systems, especially in the context of changing climatic conditions.

In Europe, the typical core altitudes of LLJs are between 140–375 m, and the typical LLJ wind speed is between 4–12 m s^{-1} (Lampert et al. 2015; Marke et al. 2018; Weide et al. 2022). This wind speed range is typically below the rated speed of wind turbines, and therefore contributes with cubic relationship to the power output. LLJ events mainly occur during the night over land, when solar energy is not available (e.g., Weide et al. 2022). Thus, wind energy generally has a larger share in the generation of renewable energy at nighttime.

Coastal areas are strongly influenced by the synoptic wind direction and the temperature difference between land and water, which leads to the formation of temperature inversions and low-level jets. During spring and summer, the surface temperature of the water is typically lower than that of the land during daytime. In addition, the aerodynamic roughness of the sea expressed in terms of the aerodynamic roughness length z_0 is several orders of magnitude smaller than the one of the surrounding land (Stull 1988). Consequently, when the flow is directed from land to sea, air masses warmed up above land are advected over the colder water surface, resulting in a pronounced temperature inversion. This phenomenon has been extensively studied for the Baltic Sea (Smedman et al. 1996; Dörenkämper et al. 2015; Svensson et al. 2016), and these flow conditions result in the development of LLJs in particular during daytime (e.g., Rausch et al. 2022). The drop in roughness at the coastline during offshore oriented wind direction enhances the LLJ formation, because it additionally contributes to the formation of a new surface layer with low turbulence intensities over the cooler ocean waters (e.g., Smedman et al. 1996). The favorable conditions for LLJ conditions, stable atmospheric stratification, have important implications for wind energy, as wakes behind wind farms decay much slower under stable conditions (Cañadillas et al. 2020) and reduce the available wind resource for downwind wind farms (Platis et al. 2020). LLJ phenomena can change the horizontal distribution of wind speed, as they are more pronounced at the

coast than above open water, and may introduce effects like the decrease of wind speed with distance from the coast (Djath et al. 2022).

With the increasing share of power production by wind energy, the forecast and control of power output on time scales of hours to days are becoming increasingly important (Veers et al. 2019). As the LLJ occur frequently and often persist over several hours (Aird et al. 2021; Weide et al. 2022), it is important to represent them well in numerical simulations for longterm site assessment and short-term power output prediction.

However, recent model validation efforts have shown that numerical simulations with models such as the Weather Research and Forecast Model (WRF) have difficulties in correctly representing the temperature profile in stable conditions (Kilpeläinen et al. 2012; Sandu et al. 2013; Siedersleben et al. 2018). For the Baltic Sea, an intercomparison of different measurement locations and four reanalyses data sets (MERRA2, ERA5, UERRA, and NEWA) with different resolutions showed a general underestimation of the LLJ wind speed (Hallgren et al. 2020), which is most probably related to too high minimum levels of turbulence in the numerical models as described by Sandu et al. (2013). The occurrence of LLJ events was best reproduced by UERRA (Hallgren et al. 2020). A recent intercomparison of LLJ radiosonde data and ERA5 reanalyses for the Arctic showed that the simulation data were able to represent reasonably well the LLJ occurrence and the LLJ wind speed, but strongly overestimate the altitude of the LLJ (López-García et al. 2022).

Furthermore, LLJ wind profiles also interact with and are modified by offshore wind park wakes (Larsén & Fischereit 2021). Increased wind shear and turbulence associated with the jets may sometimes counteract wake development (Doosttalab et al. 2020).

The following open research questions relevant for wind parks in the coastal area of the German Bight are investigated with a high resolution data set for a time period of interest for offshore wind energy are investigated here:

- How does LLJ occurrence change with distance from the coast line in the German Bight?
- During which time of day and season is LLJ occurrence most pronounced?
- Is the occurrence of LLJ particularly enhanced for offshore wind directions, with warm air masses advected from land to the colder sea?

This article, which is one of two accompanying papers, presents a comprehensive analysis of the spatial distribution of low-level jet occurrences in the German Bight. The analysis is based on an exceptionally high resolution data set that provides a detailed spatial representation of the coastal areas. This is of particular importance due to the plans for drastically increasing offshore wind parks in the near future. For example, the aim of Germany is to raise the installed capacity from 7.7 GW in 2022 to 30 GW in 2030 and even 70 GW in 2045. For the first time, the analyses extract the wind directions that are most strongly influenced by the coastal effect, which are wind directions from the South (S), South East (SE), and East (E), and compare statistics of the low-level jet occurrence to the entire dataset. The partner paper (Barekzai et al. 2024) has a specific focus on the modification of the wind field due to the coastal effect.

In this article, the introduction of the model setup is provided in Sect. 2, with a definition of the conditions for identifying LLJ events, a description of the concept of transect analysis, and an assessment of the performance of the simulation experiments. Sect. 3 provides statistical analyses of LLJ occurrence depending on season, wind direction, and distance from the coast. In Sect. 4, the results are discussed, and conclusions are drawn for the impact of LLJs on wind parks in the German Bight.

2 Methods

2.1 WRF setup

For well resolving coastal effects, the analyses were done based on a 12-year dataset of numerical simulations using the version 4.2.1 of the Weather Research and Forecast Model (WRF) with a horizontal resolution of 2 km, developed by the National Center of Atmospheric Research (Skamarock et al. 2019). The WRF model is widely used in the wind energy research community, e.g. for the generation of wind atlases (Hahmann et al. 2020; Dörenkämper et al. 2020), analysis of specific conditions (Dörenkämper et al. 2015), gap filling (Gottschall & Dörenkämper 2021) and for wind farm wake analyses (Siedersleben et al. 2018; Pryor et al. 2019; Cañadillas et al. 2022).

The study by Hahmann et al. (2020) provides a comprehensive overview of the model's sensitivities and serves as a basis for the setup used in this study that was further optimized based on experiences of modelling the North Sea offshore wind climate (e.g., Gottschall & Dörenkämper 2021; Cañadillas et al. 2022).

A nested domain approach was used, with resolutions of 18 km, 6 km and 2 km, to reduce the computational cost. The further optimization was based on offshore mast measurements, which led, for instance, to using a different nudging approach: grid nudging instead of the spectral one in NEWA. Another difference is the 2 km instead of 3 km (NEWA case) horizontal resolution. The setup was validated further offshore in the presence of wakes in (Cañadillas et al. 2022). Fig. 1 shows the distribution of the simulation domains. The boundary conditions for atmospheric variables were prescribed using the ERA5 data set (Hersbach et al. 2020) with $0.25° \times 0.25°$ (≈ 30 km) spatial resolution and 6-hour temporal resolution. Grid nudging on wind speed, temperature and humidity was applied only on the outermost (D01) domain above the 20th model level. In addition, a model option was selected to apply the grid nudging only above the boundary layer height in cases it falls above the 20th level. The six-

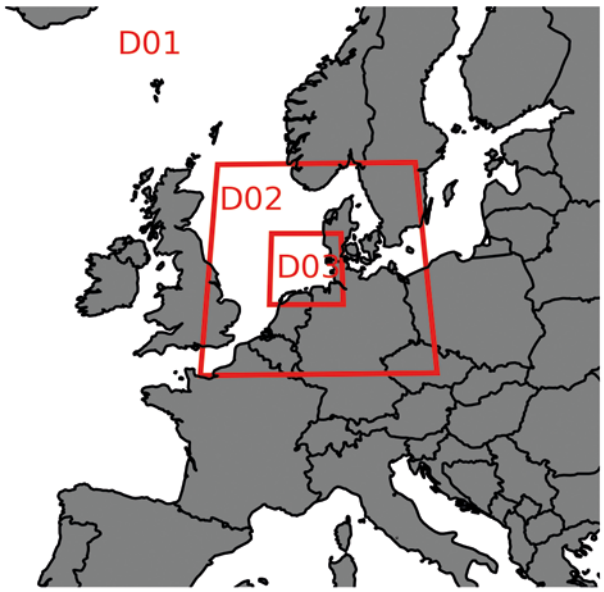

Fig. 1. Domain configuration of the WRF setup. The domains D1, D2, and D3 have a horizontal resolution of 18 km, 6 km, and 2 km, respectively.

hourly nudging on the coarsest domain above the boundary layer on the one hand keeps the downscaled wind fields close to the reanalysis, on the other hand it allows the mesoscale model's physics to develop. For the sea surface variables, the OSTIA dataset was used (Donlon et al. 2012) with 0.05° × 0.05° (≈ 6 km) spatial resolution on daily averages.

The setup used 61 vertical levels, with a dense distribution of levels across the rotor disc. The post-processed vertical levels from the dataset are 25 m, 50 m, 75 m, 90 m, 100 m, 125 m, 150 m, 175 m, 200 m, 250 m, 300 m, 350 m, 400 m, 500 m, and 1000 m. The temporal resolution of the dataset is 10 min. The setup is based on several years of experience focussing on wind energy applications (e.g. Dörenkämper et al. 2015; Hahmann et al. 2020; Dörenkämper et al. 2020; Gottschall & Dörenkämper 2021).

Roughness changes are accounted for in the WRF model by different land-use characteristics that besides other varying surface parameters also come along with a different roughness length. Above the sea the roughness length varies according to the Charnock relation and is estimated as a function of the mean wind speed (Charnock 1955). Accordingly, the Charnock coefficient is a constant for a given wind speed. However, it is known that the Charnock coefficient can be significantly affected by the wave state (Li et al. 2021). A wave model was not implemented in this study, as it is assumed that the wave effects should be very small at the altitudes studied. Dörenkämper et al. (2015) give an example on how roughness changes are treated and what flow features can result from this.

Table 1. Relevant parameters of the mesoscale model set-up. The references for the different schemes and models are summarized in WRF Users Page (2020).

Parameter	Setting
WRF model version	4.2.1
Planetary Boundary Layer (BLH) scheme	MYNN level 2.5
Land use data	MODIS
Surface layer scheme	MYNN
Microphysics scheme	WRF Single-Moment 5-class
Shortwave and long-wave radiation	RRTMG
Atmospheric boundary conditions	ERA5
Sea surface conditions	OSTIA
Horizontal resolution	18 km, 6 km, 2 km
Vertical resolution	60 eta-level
Nudging	grid nudging above BLH
Model output interval	10 min
Nesting	one-way
Land surface model	Unified Noah Land Surface Model
Duration of individual simulation	240 (+24 spin-up) hours

A summary of the model configuration decisions is provided in Table 1. A 12-year period from 2010 to 2021 was simulated, covering the period of wind farm operation in the German Bight since the erection of the first offshore wind farm alpha ventus. Compared to the New European Wind Atlas (Hahmann et al. 2020; Dörenkämper et al. 2020) with a spatial resolution of 3 km times 3 km and a temporal resolution of 30 min, covering a time period from 1989 to 2018, the WRF setup here has a higher spatial and temporal resolution, and covers a more recent time period of 12 years.

The WRF performance was evaluated with respect to wind measurements for an altitude of 100 m at two locations in the area of interest, as reported by Cañadillas et al. (2023): For the coastal area, represented by the island of Norderney, the correlation coefficient r between a wind lidar and WRF for a one-year data set (taking into account wind from South) was r = 0.85. For a four-year data set of wind speed measurements at the offshore site FINO1 (wind from South), the correlation coefficient was r = 0.84

A dedicated WRF sensitivity study for the Baltic Sea indicates an underestimation of the LLJ strength, particularly for very stable conditions; it was therefore important to include information on both land and sea surface (Li et al. 2021b), which was taken into account for this study.

2.2 Detection of low level jets

Low-level jets are known to exhibit highly variable characteristics, and a strict definition of the phenomenon remains elusive. It is currently proposed that LLJ events may be defined via wind shear rather than a fixed threshold for the decrease of wind speed (Hallgren et al. 2023), or using site-specific values for threshold wind speed or wind shear (Hallgren et al. 2023). In particular for numerical simulations, which have generally smoother profiles than experimental data sets, a lower threshold is frequently used. E.g. Hallgren et al. (2020) used a criterion of 1 m s^{-1}, for assessing the performance of MERRA2, ERA5, UERRA, NEWA in representing LLJ in comparison with lidar, and Rubio et al. (2022) and Ziemann et al. (2020) used a criterion of 0.5 m s^{-1} and a ratio of at least 1.05 between the wind speed at the jet core height v_{max} and the subsequent minimum wind speed v_{min}, called in the following peak prominence. Kalverla et al. (2020) compared the ability of three wind atlases to represent the LLJ measured at the meteorological mast Ijmuiden off the Dutch coast based on a criterion of 2 m s^{-1}, and the wind atlas with the highest spatial resolution of 2.5 km, the Dutch Offshore Wind Atlas (DOWA), resulted in the best identification of LLJ events compared to the observations. Global classifications of LLJ events with a criterion of 2 m s^{-1} fail to include the North Sea entirely, compared to stronger coastal LLJ events at the west coast of the continents (Luiz & Fiedler 2024). Generally, the identification of LLJ events is highly sensitive to the applied criteria for LLJ detection (Rubio et al. 2022), with lower absolute or relative thresholds resulting in more LLJ events, and on average lower wind speed, but similar jet core height (Aird et al. 2021). Further, there is a large effect of the height interval taken into account for applying the LLJ criteria (Kalverla et al. 2019), and the vertical resolution of the data has a high impact on the frequency of occurrence, the peak prominence and altitude of the LLJ (Aird et al. 2021). For the purpose of this study, an LLJ is defined as a maximum in the wind profile with a low peak prominence (*pp*) of at least 0.25 m s^{-1} compared to the wind speed minimum above, as illustrated in Fig. 2. The maximum search height for the minimum is 1 km. If there are two minima, only the lower one is taken into account. This includes also LLJ events for very low peak prominence for two reasons: First, the LLJ strength above the North Sea is smaller compared to onshore sites, and including these events provides a larger data base, which is then subdivided into events occurring for different wind directions. A change in the LLJ criterion from 0.25 m s^{-1} to the typically applied criterion of 2 m s^{-1} would result a loss of approximately 57% of the LLJ events, in particular above the North Sea. Second, the aim of the article is to understand the horizontal variability of LLJ events in the area of the coastal transition, where the values of LLJ strength do not play a major role, without the intention to compare to other sites. The *pp* is calculated as the difference between the maximum wind speed of the jet core and the baseline wind speed given by the wind speed

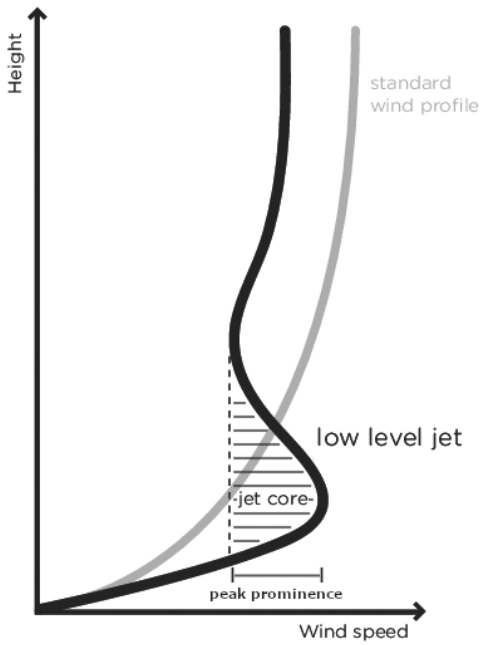

Fig. 2. A sketch of a standard wind profile (power law or logarithmic, gray line) and a low level jet wind profile (black line). The area between the dashed line drawn down from the wind speed minimum above the jet and the LLJ maximum is termed jet core and describes the vertical position of the jet. The wind speed difference between the dashed line and the jet maximum is termed peak prominence (based on Fig. 3 in (Hallgren et al. 2020)).

minimum above the jet. In the analysis, the *pp* is not only calculated for the height of the maximum, but also over the vertical range with enhanced wind speed compared to the baseline (see Fig. 2). The vertically resolved LLJ distribution is normalized to the wind speed maximum, enabling the evaluation of LLJ characteristics over ranges of heights. This approach differs from the definition of an LLJ in Lampert et al. (2015); Kalverla et al. (2019), where an LLJ is defined as a wind maximum below an altitude of 500 m with a peak prominence of at least 2 m s^{-1} and a ratio of 25% between the wind speed maximum and minimum. This definition is adequate for atmospheric profiles measured by LIDAR, but the WRF simulation results are smoother, allowing for a more inclusive LLJ criterion (e.g., 0.5 m s^{-1} in Ziemann et al. 2020). Moreover, the simulations capture the LLJ's horizontal extent, which can span over large distances and therefore many square kilometers (Rausch et al. 2022) and model grid cells. The analysis focuses on two LLJ characteristics: LLJ peak prominence (*pp*) and LLJ probability (P_{LLJ}). P_{LLJ} is calculated by normalizing the *pp* at the jet core to 1, resulting in the vertical distribution of the low-level jet. The number of LLJs (n_{LLJ}) vertically integrated between an altitude of 0 m and 200 m or 500 m, and measured over a certain time interval, is determined using Equation 2.1. Finally, the LLJ probability P_{LLJ} is calculated integrating the number of LLJs ($\tilde{n}_{LLJ}$) over a certain time interval Δt_{step} proportional to the number of evaluated time steps (n_t), see Equation 2.2.

$$n_{LLJ} = \tilde{n}_{LLJ}\,\Delta t_{step} = P_{LLJ}\,\Delta t_{tot} = P_{LLJ}\,n_t\,\Delta t_{step} \quad (2.1)$$

$$P_{LLJ} = \tilde{n}_{LLJ} / n_t \quad (2.2)$$

2.3 Transect analysis

The wind speed datasets were divided into wind direction sectors of 45 degrees, as illustrated in the wind rose in Fig. 3. For the whole dataset and a subset containing only the three wind directions originating from land and blowing over the North Sea, namely S, SE and E, collectively referred to as "offshore" wind directions, several parallel transects of 50 km width were defined along each direction, labeled as S1–3, SE1–4 and E1–5 (see Figs. 4 and 5). The grid cells encompassed within the transects were analyzed as follows: for each transect, the atmospheric variables were averaged perpendicular to the alignment of the transect. These averages were then combined by taking the mean of the parallel transects, and the standard deviation was determined. This means that for taking into account the whole data set, the standard deviation is much lower than for only specific wind directions. The transects were aligned based on the average position of the coastal transition of the respective transect. This approach enables the investigation of the horizontal development of the atmospheric boundary layer and specifically the wind profile with fetch length, based on statistically representative data sets. To carry out the analysis, the data set was filtered by principal wind direction (E, SE, S), height (100 m, 200 m, 300 m), individual years between 2010 and 2021, seasonal changes, and day and nighttime.

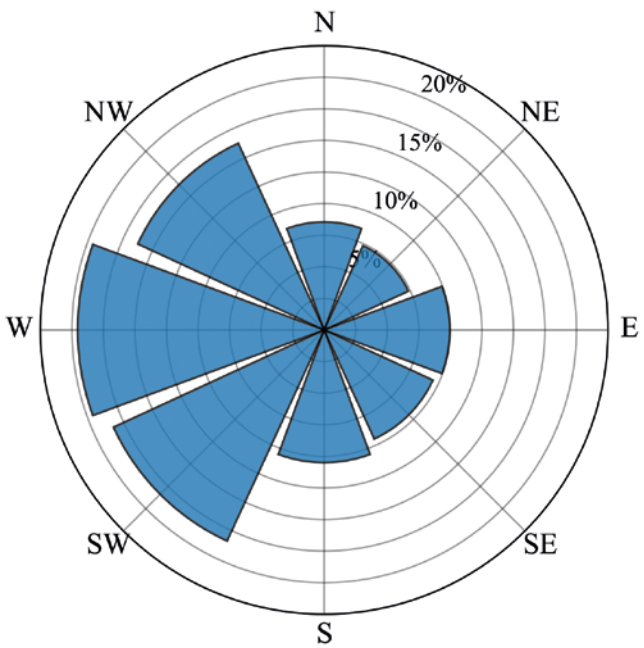

Fig. 3. The WRF wind rose shows the distribution of modelled wind directions for the 12-year period from 2010 to 2021, partitioned into eight compass directions. The results are evaluated below a height of 200 m and over the area with the corner coordinates latitude ∈ (54, 55) and longitude ∈ (6, 8). Each circle represents an occurrence of 2.5%.

3 Results

In this section, different low-level jet characteristics are analyzed in relation to the prevailing wind direction. To analyze the influence of offshore versus onshore wind directions, the three offshore wind directions South (S), Southeast (SE), and East (E) are grouped together. The statistics of low-level jets are calculated in the region of the German Bight, as shown in Fig. 4. Furthermore, the datasets were divided per season according to months in the following way: winter (Dec, Jan, Feb), spring (Mar, Apr, May), summer (Jun, Jul, Aug) and autumn (Sep, Oct, Nov). For day and night-time the dataset is divided using the definition of true sunrise and sunset for each day of the year with the center of the WRF domain as reference location and within the 10 min temporal resolution. The average wind direction is calculated over an area given by the domain center between 7° and 8° latitude, 53.5° and 54.5° longitude and evaluated below an altitude of 200 m. Fig. 3 presents the relative frequencies of these wind directions over the German Bight. The data were obtained from 12 years of simulation results, which show that the offshore wind directions together have a frequency of approximately 30% in the German Bight.

3.1 Spatial distribution of LLJ occurrence in the German Bight

Fig. 4 displays the spatial distribution of the probability of a low-level jet P_{LLJ}, integrated below a height of 200 m, averaged over the 12-year period. The integrated time intervals are classified by wind direction, including all directions (Fig. 4a), E (Fig. 4b), S (Fig. 4c), and SE (Fig. 4d). The aerial overlays in panels b), c), and d) will be used in the subsequent transect analyses in the following sections. The LLJ probability for easterly (Fig. 4b) and south-easterly (Fig. 4d) wind directions is significantly higher than that for all wind directions (Fig. 4a). For easterly wind directions (Fig. 4b), there is a substantial increase in LLJ probability along the southern coastline, along the wind direction, with the highest LLJ probability in the South. The highest LLJ probabilities P_{LLJ} over water are close to 0.23. For south-easterly wind directions (Fig. 4d), the highest LLJ probability is shifted towards the center of the German Bight, close to the island Heligoland. Furthermore, the highest probabilities over land are found with P_{LLJ} close to 0.24. In contrast, for easterly (Fig. 4b) and south-easterly (Fig. 4d) wind directions, the LLJ probability is reduced to as low as 0.1 right downwind the easterly coastline, which is oriented approximately perpendicular to the wind direction. For southerly wind directions (Fig. 4c), there is overall less LLJ activity and therefore a less pronounced reduction in LLJ probability after the coastline perpendicular to the wind direction, and a less pro-

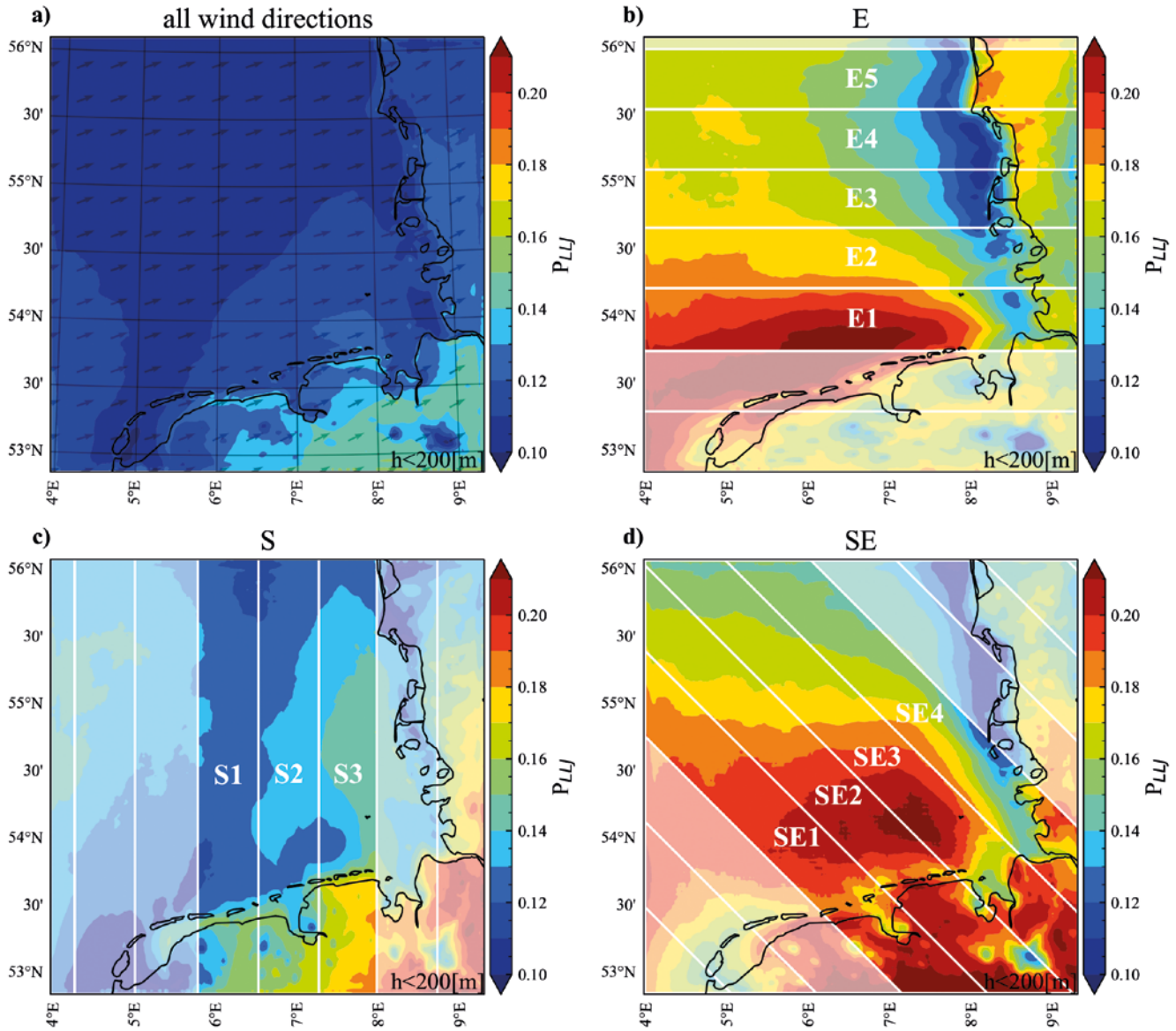

Fig. 4. The spatial distribution of the relative LLJ frequency P_{LLJ}. The results are based on WRF simulations over the German Bight, evaluated and integrated for heights below 200 m and averaged between 2010 and 2021. Panel a) is averaged over "all wind directions" (with arrows for the mean wind direction), panel b), c) and d) are evaluated for easterly "E", southerly "S" and south-easterly "SE" wind directions, respectively. The highlighted and labelled areas (S1–3, SE1–4 and E1–5) are the basis of the subsequent transect analysis.

nounced LLJ peak along the eastern coastline parallel to the wind direction. Finally, when comparing LLJ activity over land and water, southerly (Fig. 3c) and all wind directions (Fig. 4a) show more LLJ activity over land than over water, while easterly (Fig. 4b) and south-easterly (Fig. 4d) wind directions show more LLJ activity over water than over land.

Fig. 5 presents the spatial distribution of the average peak prominence of the LLJ at the height of 100 m. This figure follows the same structure as Fig. 4, and the concept of peak prominence is explained in Section 2. On average, the peak prominence is larger over land than over water. The average peak prominence for all wind directions (Fig. 5a) exhibits an area of lower peak prominence following the shoreline. The peak prominence is higher for easterly (Fig. 5b) and south-easterly wind directions (Fig. 5d) compared to the average.

For easterly wind directions, an area of enhanced peak prominence is observed offshore near the southern coast in the same region as the LLJ probability maximum (Fig. 4b). The peak prominence decreases after the shoreline along the wind direction and increases again further offshore. Southerly wind directions (Fig. 5c) show a peak prominence lower than the average over water. For south-easterly wind

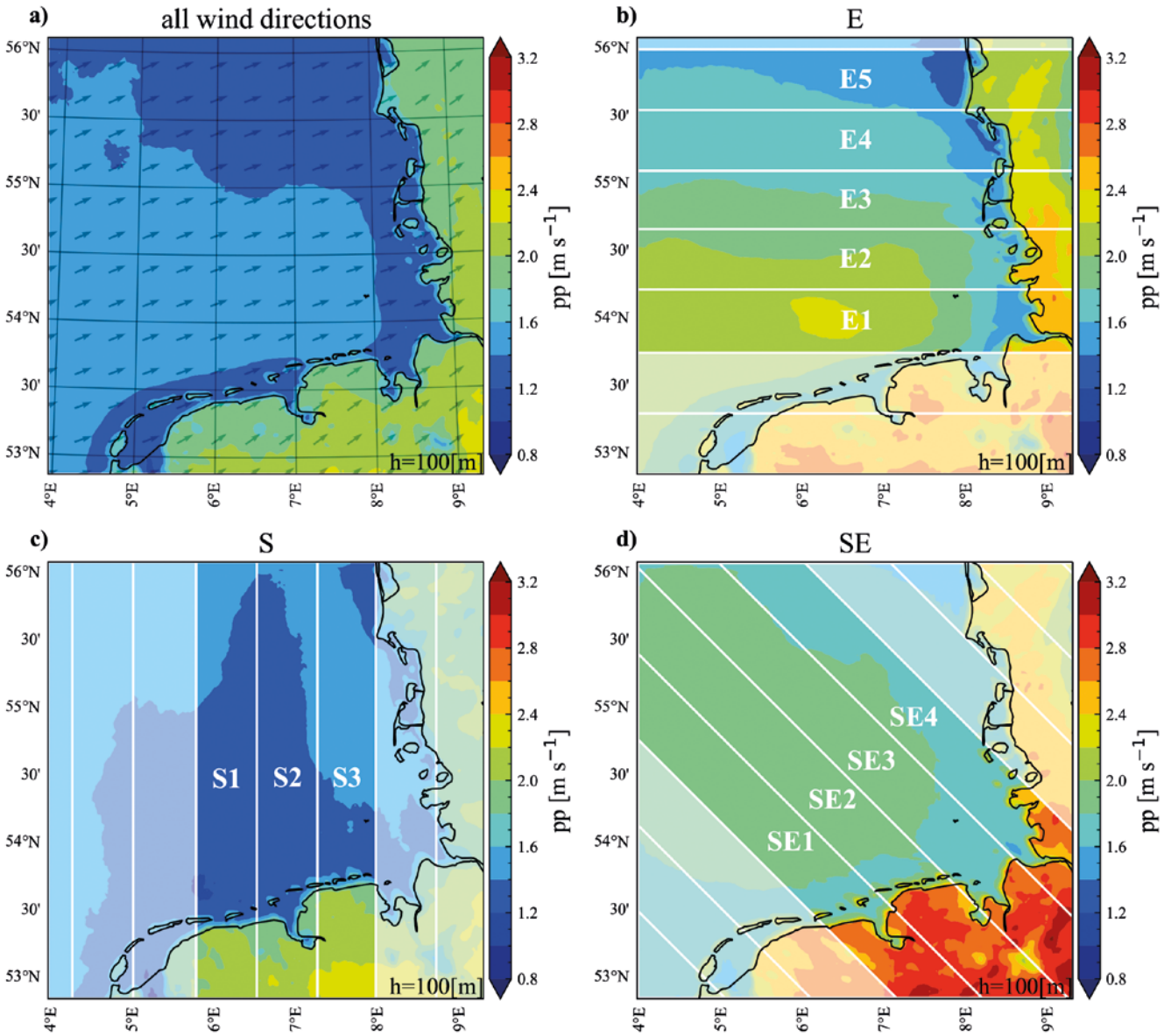

Fig. 5. The spatial distribution of the average LLJ peak prominence *pp* in m s^{-1}, evaluated at the height of 100 m. The threshold or minimum peak prominence is 0.25 m s^{-1} (further information in Fig. 4).

directions (Fig. 5d), the peak prominence is highest over land. Moreover, the peak prominence decreases after the coastline and increases again further offshore, but this effect is less pronounced than for easterly winds. In general, areas of enhanced LLJ probability also exhibit an increase in peak prominence.

3.2 Low-level jet development with fetch

Fig. 6 shows the probability of low-level jets for the transect analysis at the heights of 100 m, 200 m, and 300 m. The panels compare the results for all wind directions (Fig. 6a) with the results for offshore wind directions only (Fig. 6b). The results are averaged for easterly, southerly, and south-easterly wind directions along the transects E1–5, S1–3, and SE1–4, respectively. In the vertical direction, the results are integrated over an interval of 50 m (25 m below to 25 m above the indicated altitude). Fig. 4 shows the evaluated transect areas, and further information can be found in Sect. 2.

The LLJ probability for all wind directions (Fig. 6a) decreases after the coastal transition and levels off further offshore for all heights. The largest LLJ probability, on average, is found at a height of 200 m. The LLJ probability for all wind directions ranges from approximately 0.03 to 0.045 for all heights. The LLJ probability for offshore conditions (Fig. 6b) is higher by a factor between 1.5 and 2 than for all wind directions. The LLJ probability for offshore wind directions increases towards the coastline, decreases after the

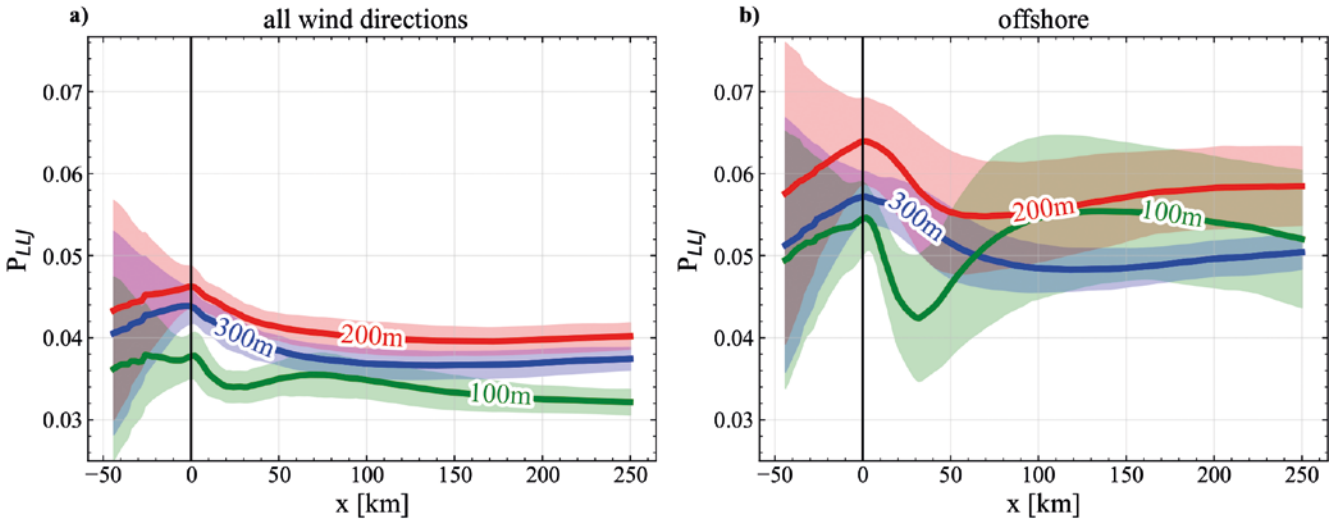

Fig. 6. Transect analysis of the LLJ probability at different heights. The results are integrated over a range of 50 m around the heights 100 m (green), 200 m (red), and 300 m (blue). The temporal averages are taken between 2010 and 2021 and spatially averaged over the transect areas shown in Fig. 4b), c) and d). Transect data is averaged, and the coastline is aligned, resulting in the spatial dimension *x*, which is negative over land and positive over water. The panel a) is averaged over all wind directions and b) is averaged only over offshore wind directions, i.e. southerly wind directions are evaluated along the transects S1, S2, S3, easterly wind directions are evaluated along E1, E2, E3, E4, E5, south-easterly wind directions are evaluated along SE1, SE2, SE3, SE4. The areas shaded in brighter color indicate the standard deviation, which is generally lower if more data are included in the statistics (in particular for the whole data set containing all wind directions).

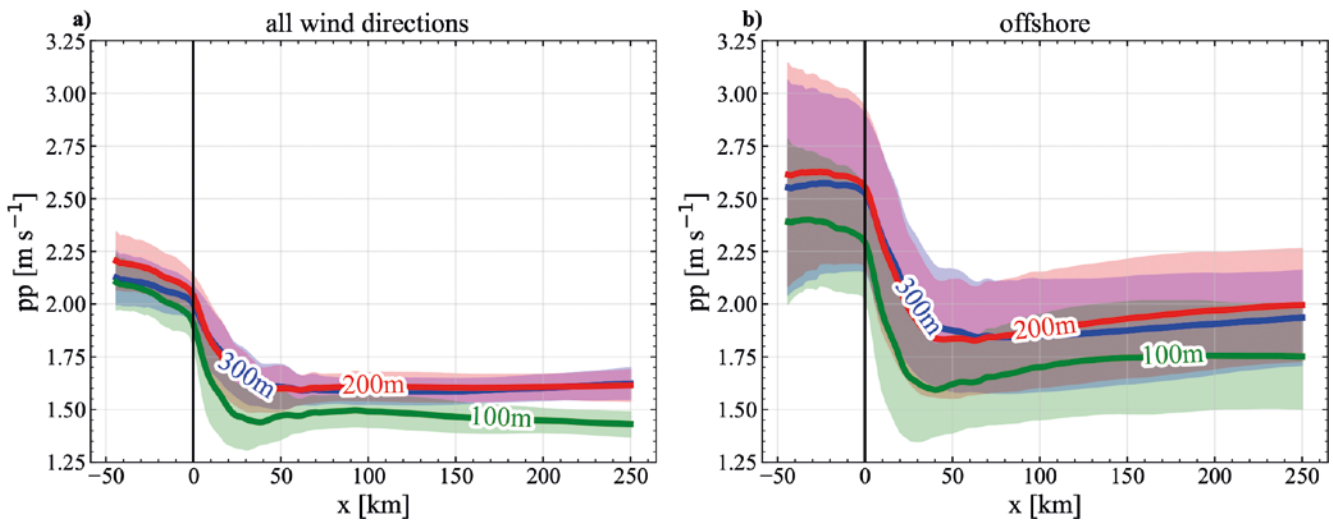

Fig. 7. Transect analysis of the LLJ peak prominence *pp*. Results are evaluated at the heights 100 m (green), 200 m (red), and 300 m (blue). LLJs are included with a minimum pp of 0.25 m s^{-1}. The areas shaded in brighter color indicate the standard deviation. The panel a) is averaged over all wind directions and b) is averaged only over offshore wind directions (more information in Fig. 6).

coastal transition, and starts increasing again at a distance of around 50 km after the coastline, above water, for all altitudes (Fig. 6a). At the height of 100 m, the LLJ probability for offshore wind directions drops from 0.06 to 0.04 after the coastal transition and recovers to a value of 0.055 after a distance of 100 km offshore (Fig. 6b). Again, the highest probability is found at the height of 200 m. The LLJ probability for offshore wind directions is approximately in the range of 0.04 and 0.065 for all heights (Fig. 6b).

Fig. 7 shows the peak prominence of the transect analysis for the heights 100 m, 200 m, and 300 m. The peak prominence is smaller if all wind directions are included in the average value (Fig. 7a), and drops off after the coastal transition from around 2 to 1.5 m s^{-1} at a distance of around 50 km offshore and stays approximately constant. For offshore wind directions (Fig. 7b), the peak prominence decreases from 2.5 to 1.75 m s^{-1} after 50 km, but increases slightly further offshore.

The highest LLJ probability and variability for offshore wind directions are observed for wind from Southeast (see Appendix, Fig. A.1). Furthermore, also the highest peak prominence is observed for wind direction from Southeast (see Appendix, Fig. A.2). For all wind directions, the LLJ probability over water is almost constant, with values between 0.03 and 0.04. Offshore wind directions show the highest LLJ probability values for the SE transect orientation (see Appendix, Fig. A.1). After a small reduction following the coastal transition, there is a peak in probability of 0.065 after a distance of 100 km offshore. The E transect orientation (see Appendix, Fig. A.1b) shows a strong reduction in probability from 0.06 to 0.038 after the coastal transition, followed by a significant increase back to 0.06 after a distance of 150 km offshore. The S transect orientation (see Appendix, Fig. A.1b) shows a strong reduction in probability after the coastal transition, from 0.06 to 0.038, followed by a gradual increase and a less pronounced peak of 0.045 after a distance of 100 km.

For all wind directions, the LLJ peak prominence decreases after the coastal transition and remains constant at around 1.5 m s^{-1}. However, for each of the three transect orientations, there is a strong drop in peak prominence after the coastal transition, followed by a constant value further offshore (see Appendix, Fig. A.2). Specifically, the E and SE orientations have a peak prominence of around 1.8 m s^{-1}, while the S orientation has a peak prominence of 1.3 m s^{-1} after a distance of 100 km offshore.

3.3 Interannual variability of low-level jets

The interannual variability of the low-level jet probability for the years 2010 to 2021 reveals that in some years, such as 2011 and 2018, there is a reduced average LLJ frequency near the coast, but an increased probability with a maximum approximately at a distance of 75 km from the coast (see Appendix, Fig. A.3). For offshore wind directions, a relatively uniform development of the LLJ probability with distance is observed, but the probabilities of the individual years differ in how much they decrease after the coastal transition and how much they increase after approximately 100 km over the water. The range of LLJ probability occurrence found for a distance beyond 100 km offshore is between 0.045 and 0.065. The years of 2013 and 2021 show the lowest LLJ probability for offshore wind directions. The interannual variability of the LLJ peak prominence development with fetch is qualitatively similar for all wind directions and offshore wind directions only (see Appendix, Fig. A.4). The peak prominence for offshore wind directions is enhanced by approximately 0.2 m s^{-1}, with a higher variability.

3.4 Seasonal and diurnal variability of low-level jets

The seasonal and diurnal variability of LLJ occurrence are shown in the Fig. 8 and 9. The results indicate that the frequency of low-level jets is generally higher for offshore wind directions compared to all wind directions, both above land and water (Fig. 8). Additionally, the LLJ frequency increases from land to water during spring and summer. The LLJ frequency is most pronounced for offshore wind directions during spring and summer, therefore for stable conditions with colder water surface and warmer advected air masses. Conversely, autumn and winter have a much lower LLJ probability above water, with the LLJ frequency decreasing from land to water. The largest LLJ frequencies are recorded during summer days at 100 m height, with a value of 0.1.

Concerning the diurnal LLJ probability, a similar development is observed for day time (Fig. 9), namely a strong increase of LLJ probability with distance to the coast. For night time, the overall LLJ probability is enhanced for all distances for offshore wind directions compared to all wind directions, with highest LLJ probability above land.

The LLJ peak prominence is most pronounced above water during spring and summer days for offshore wind directions, and above land during spring and summer nights (not shown).

4 Discussion and conclusions

Although the LLJ statistics are not directly comparable to other studies with different LLJ criteria, the general features can be compared. LLJ were more frequently observed above land than above sea, which is in agreement with previous findings (Tuononen et al. 2015). The WRF studies confirm that low-level jet events occur more frequently during stable conditions, as shown by Rausch et al. (2022), which depend on wind directions (Schulz-Stellenfleth et al. 2022), times of day (Rausch et al. 2022), and seasons (Hallgren et al. 2020). LLJs are most common over water for offshore wind directions in spring and summer during the day, when warmer air masses from land are advected over colder water surfaces (Schulz-Stellenfleth et al. 2022). Also the study of Wagner et al. (2019) identified most LLJ events at the meteorological mast FINO1 for wind directions from the sector East to South. For all wind directions, LLJ occurrence is enhanced over land during the night, which corresponds to the formation of a temperature inversion due to nocturnal cooling, a phenomenon that is generally observed for onshore sites (Lampert et al. 2015). The peak prominence for different seasons, wind directions, and times of day is generally higher over land than over water. It is important to note that the wind speed is generally higher over water, which is not taken into account in the definition of peak prominence in this article. Normalizing to a reference wind speed would further decrease peak prominence over water.

The studies confirm the significance of LLJ events for coastal wind energy, which extends beyond just a few kilometers from the coast. This is consistent with frequent observations of LLJ occurrences at offshore sites, such as meteorological towers (Kalverla et al. 2019) and at the island

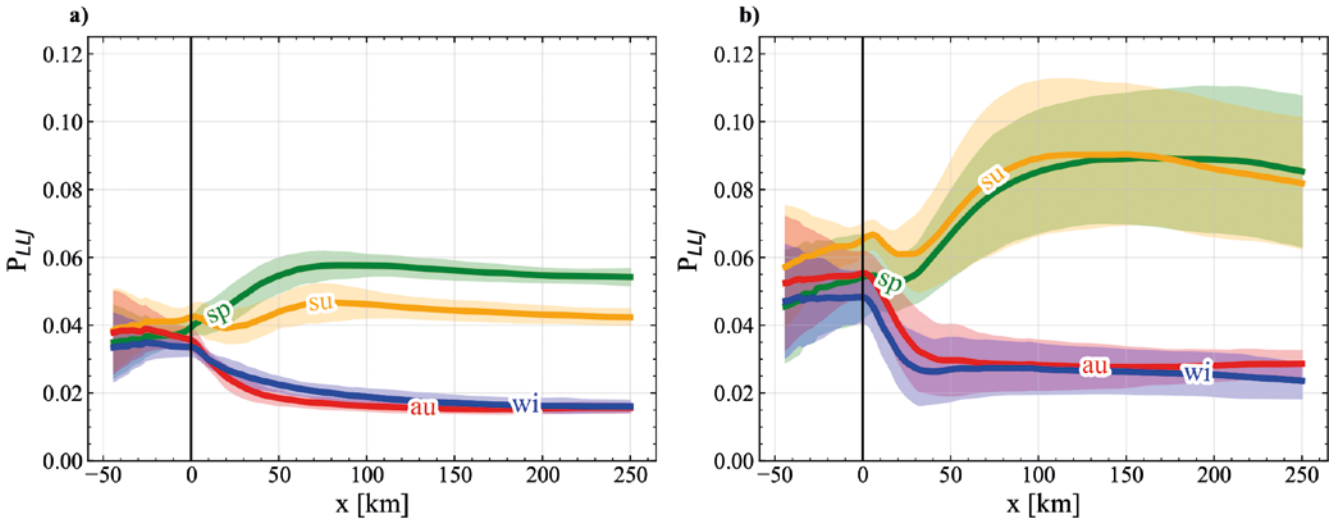

Fig. 8. The seasonal variability in the LLJ probability integrated over a height range of 50 m around the height of 100 m, from 2010 until 2021. Panel a) is averaged over all wind directions, and panel b) is averaged only over offshore conditions. The colours represent the different seasons, spring (green), summer (yellow), autumn (red) and winter (blue).

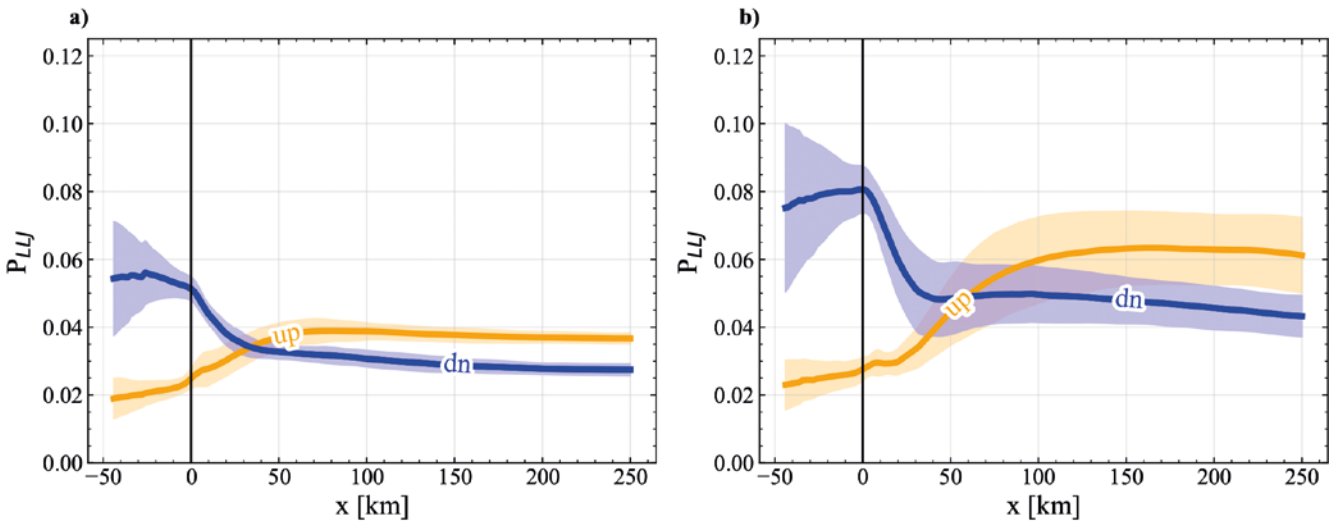

Fig. 9. The diurnal variability in the LLJ probability integrated over a height range of 50 m around the height of 100 m, from 2010 until 2021. Panel a) is averaged over all wind directions, and panel b) is averaged only over offshore conditions. Night time (sun down) data are shown in blue, day time (sun up) in yellow.

of Heligoland (Rausch et al. 2022). With peak prominence of LLJs typically ranging from 1 to 3 m s^{-1} for offshore wind directions and an enhanced LLJ occurrence extending more than 50 km downstream, particularly during the daytime of spring and summer, the phenomenon should be taken into account in wind potential assessments, in particular as LLJs strongly interact with wind park wakes that reach far downstream, depending on the jet core height (Gadde & Stevens 2021).

In conclusion, the WRF analyses provide the following answers to the research questions formulated in Sect. 1:

- On average, LLJ events can be expected most frequently at the coast, with generally decreasing probability of occurrence with distance from the coast. However, for offshore wind directions, the LLJ frequency of occurrence is enhanced both above land and above open water, with lower LLJ probability directly at the coastal transition, but an increase up to large distances of more than 100 km.
- LLJ events above the German Bight occur most frequently during spring and summer, and during day time.
- LLJ occurrence above the German Bight is strongly related to wind direction, and is enhanced for wind directions advecting warmer air masses from land over sea with colder surface temperature.

The results are in agreement with other studies, and in addition provide a clear picture of spatial distribution of the LLJ occurrence for the whole area of the German Bight.

Acknowledgments: This work was performed as part of the project X-Wakes funded by the German Federal Ministry of Economic Affairs and Energy (BMWi), now Federal Ministry for Economic Affairs and Climate Action (BMWK) under grant number FKZ 03EE3008 on the basis of a decision by the German Bundestag. The authors would like to thank the partners of X-Wakes for the fruitful discussions.

A Appendix

In the following, additional graphics are provided for more detailed studies of the variability between transects concerning LLJ probability (Fig. A.1) and LLJ peak prominence (Fig. A.2), and the interannual variability of LLJ probability (Fig. A.3) and LLJ peak prominence (Fig. A.4).

Fig. A.5 and Fig. A.6 present a comprehensive overview of all experiments, including the distinction between all and only offshore wind directions, day and night, and the four seasons.

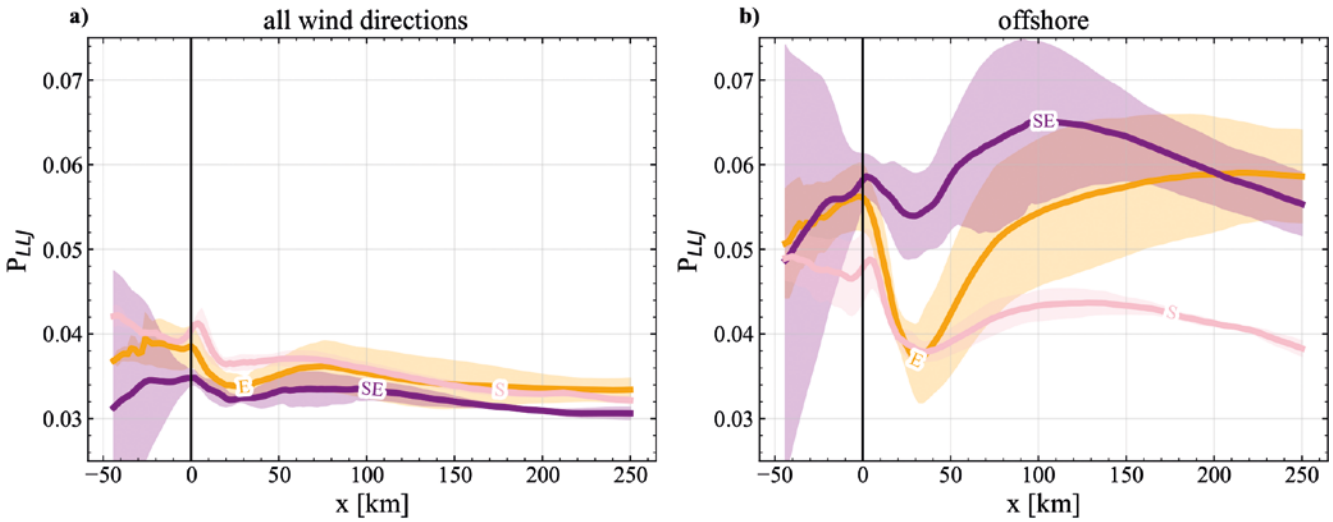

Fig. A.1. The variability between transects in the LLJ probability is integrated over a 50 m strip around the height of 100 m for the alignment of the transects along E (orange), SE (violet) and S (rose). The transects areas are shown in Fig. 4 panel b), c) and d). The panel a) is averaged over all wind directions and panel b) contains only over offshore conditions. The areas shaded in brighter color indicate the standard deviation.

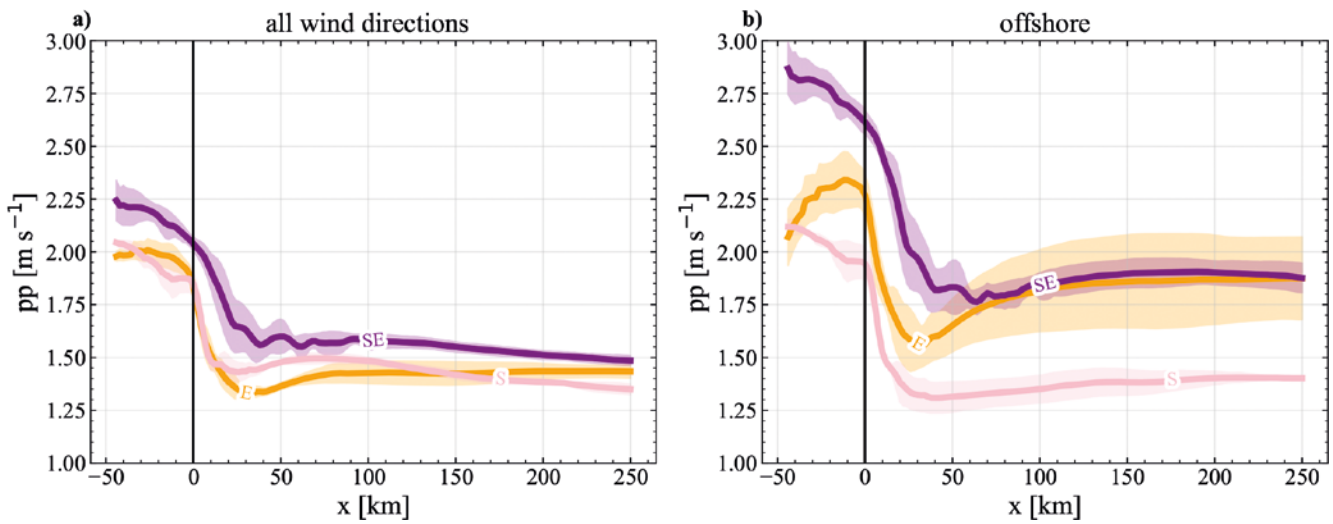

Fig. A.2. The variability between transects of LLJ peak prominence *pp* evaluated at a height of 100 m for the alignment of the transects along E (orange), SE (violet) and S (rose). The transects areas are shown in Fig. 4 panel b), c) and d). The panel a) is averaged over all wind directions and panel b) is averaged only over offshore conditions. The areas shaded in brighter color indicate the standard deviation.

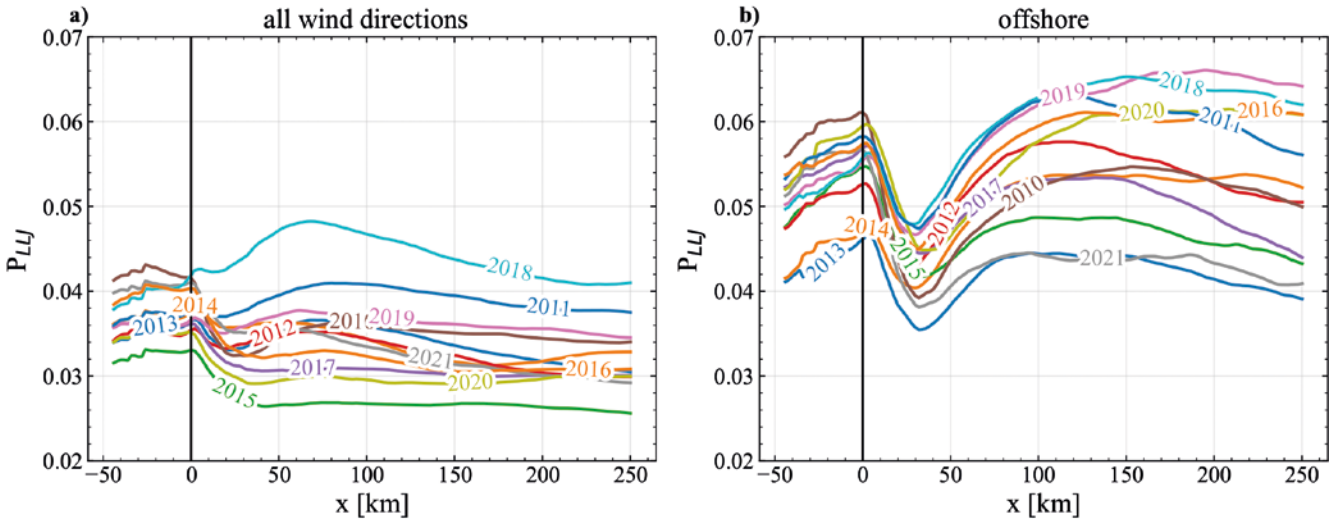

Fig. A.3. The interannual variability in the LLJ probability integrated over a stripe of 50 m around the height of 100 m, from 2010 until 2021. Panel a) is averaged over all wind directions, and panel b) is averaged only over offshore conditions.

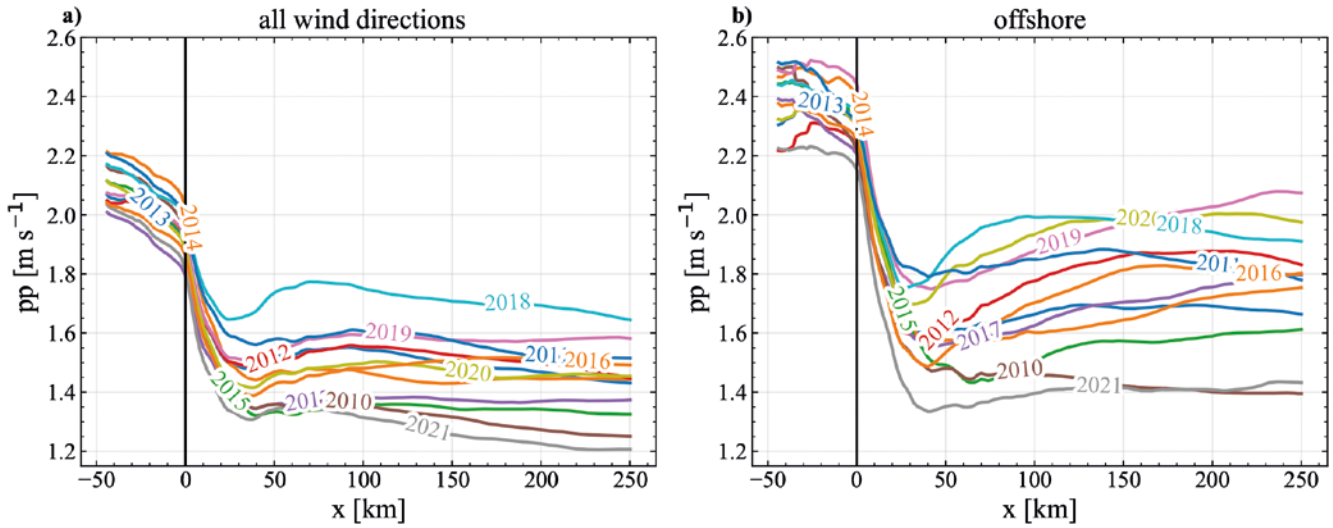

Fig. A.4. The interannual variability LLJ peak performance *pp* evaluated at a height of 100 m from 2010 until 2021. The panel a) is averaged over all wind directions and panel b) is averaged only over offshore conditions.

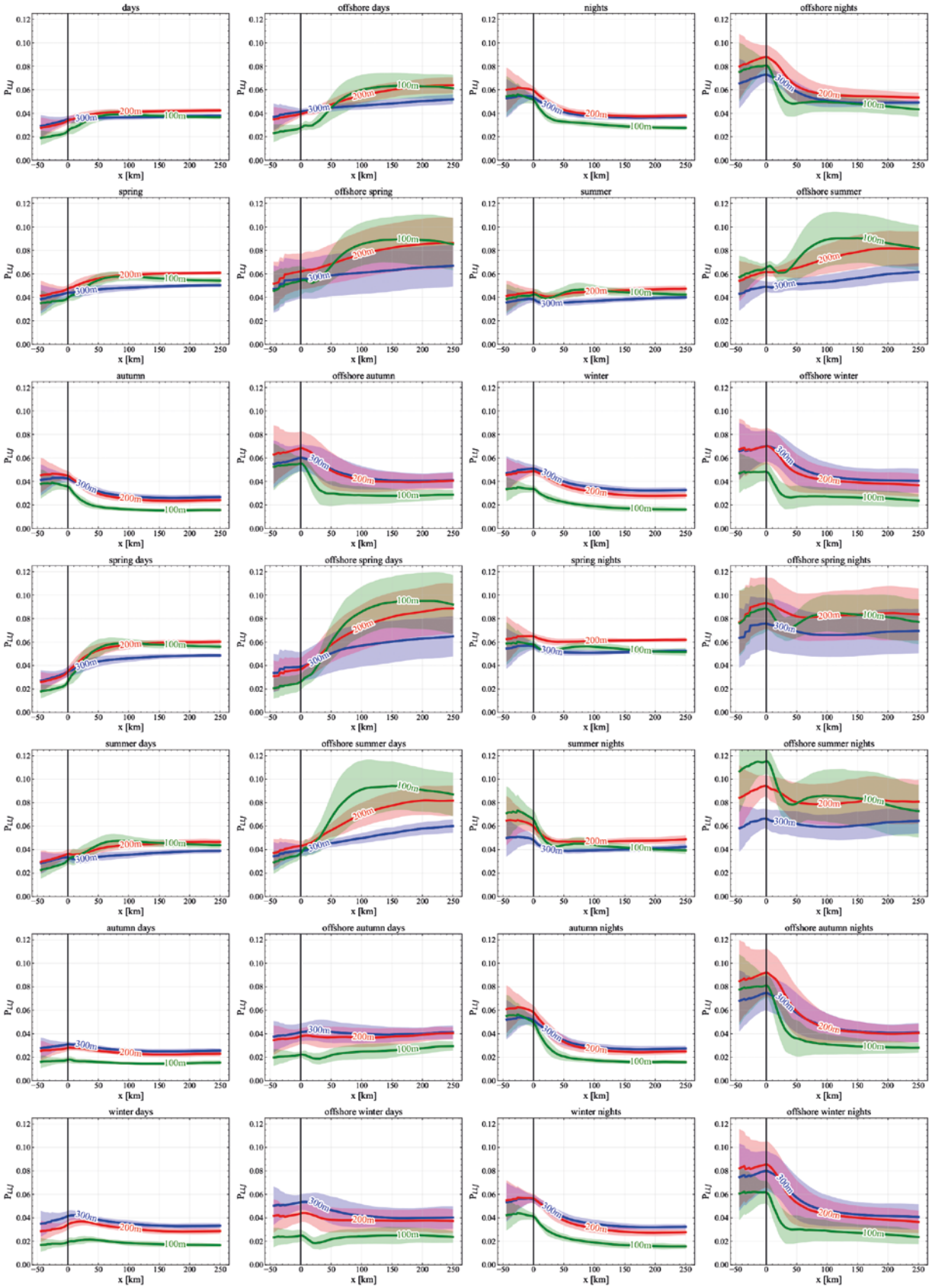

Fig. A.5. A summary of the all experiments showing the LLJ probability for different altitudes (100 m green, 200 m red, 300 m blue). The areas shaded in brighter color indicate the standard deviation (further information in Fig. 6).

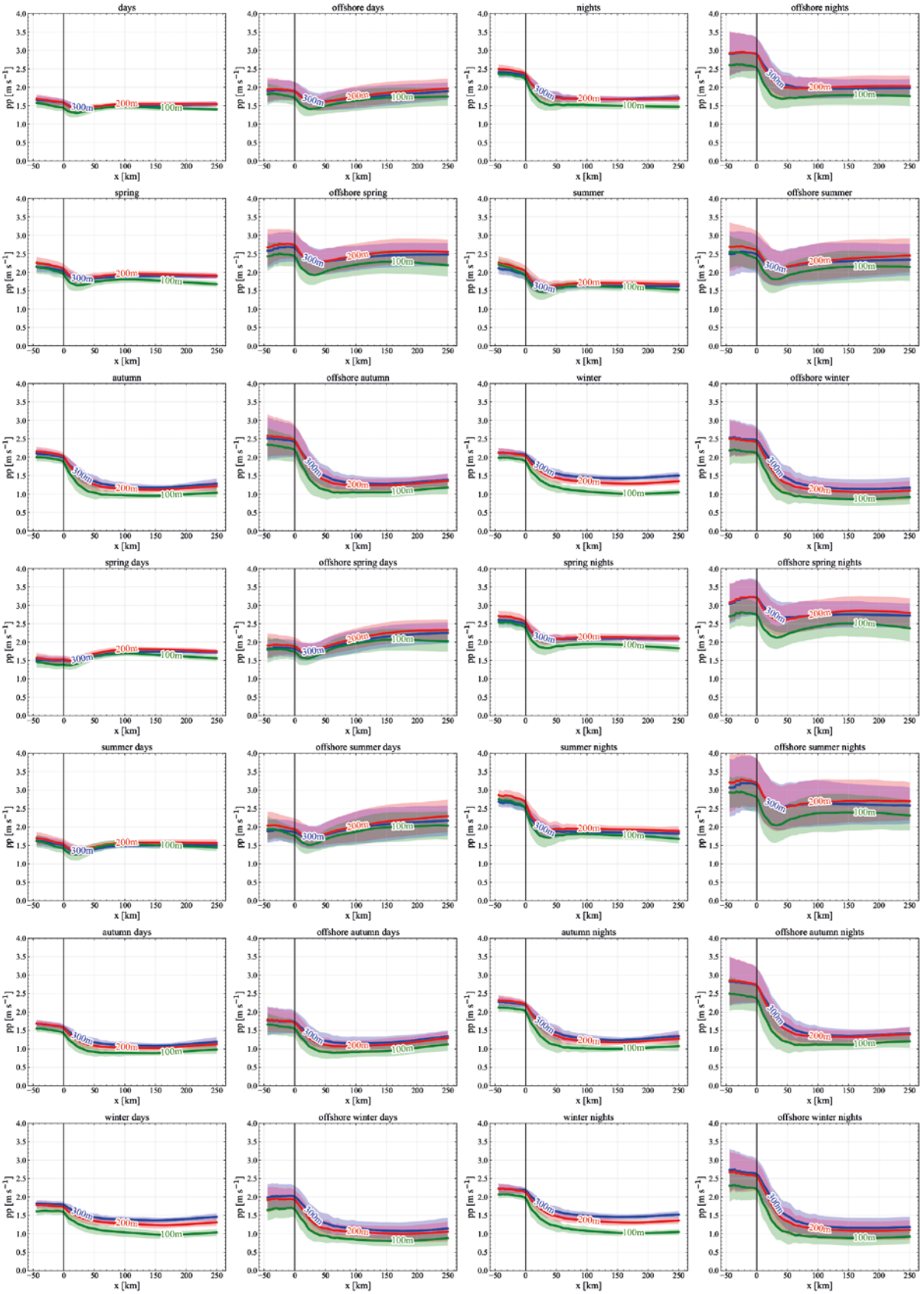

Fig. A.6. A summary of the all experiments showing the LLJ peak prominence *pp*. (100 m green, 200 m red, 300 m blue). The areas shaded in brighter color indicate the standard deviation (further information in Fig. 6).

References

Aird, J. A., Barthelmie, R. J., Shepherd, T. J., & Pryor, S. C. (2021). Wrf-simulated low-level jets over iowa: Characterization and sensitivity studies. *Wind Energy Science, 6*(4), 1015–1030. https://doi.org/10.5194/wes-6-1015-2021

Andreas, E., Claffy, K., & Makshtas, A. (2000). Low-level atmospheric jets and inversions over the western weddell sea. *Boundary-Layer Meteorology, 97*(3), 459–486. https://doi.org/10.1023/A:1002793831076

Baas, P., Bosveld, F., Klein Baltink, H., & Holtslag, A. (2009). A climatology of nocturnal low-level jets at cabauw. *Journal of Applied Meteorology and Climatology, 48*(8), 1627–1642. https://doi.org/10.1175/2009JAMC1965.1

Barekzai, M., Cañadillas, B., Emeis, S., Dörenkämper, M., & Lampert, A. (2024). (in review). Analysis of 12-year wrf simulations for the coastal area of the german bight – part 2: Impact of the coastal transition on the offshore wind speed development. *Meteorologische Zeitschrift.*

Blackadar, A. K. (1957). Boundary-layer wind maxima and their significance for the growth of nocturnal inversions. *Bulletin of the American Meteorological Society, 38*(5), 283–290. https://doi.org/10.1175/1520-0477-38.5.283

Cañadillas, B., Foreman, R., Barth, V., Siedersleben, S., Lampert, A., Platis, A., … Neumann, T. (2020). Offshore wind farm wake recovery: Airborne measurements and its representation in engineering models. *Wind Energy, 23*(5), 1249–1265. https://doi.org/10.1002/we.2484

Cañadillas, B., Wang, S., Ahlert, Y., Djath, B., Barekzai, M., Foreman, R., & Lampert, A. (2023). Coastal horizontal wind speed gradients in the north sea based on observations and era5 reanalysis data. *Meteorologische Zeitschrift, 32*(3), 207–228. https://doi.org/10.1127/metz/2022/1166

Cañadillas, B., Beckenbauer, M., Trujillo, J. J., Dörenkämper, M., Foreman, R., Neumann, T., & Lampert, A. (2022). Offshore wind farm cluster wakes as observed by long-range-scanning wind lidar measurements and mesoscale modeling. *Wind Energy Science, 7*(3), 1241–1262. https://doi.org/10.5194/wes-7-1241-2022

Charnock, H. (1955). Wind stress on a water surface. *Quarterly Journal of the Royal Meteorological Society, 81*(350), 639–640. https://doi.org/10.1002/qj.49708135027

Davies, P. A. (2000). Development and mechanisms of the nocturnal jet. *Meteorological Applications, 7*(3), 239–246. https://doi.org/10.1017/S1350482700001535

Djath, B., Schulz-Stellenfleth, J., & Cañadillas, B. (2022). Study of coastal effects relevant for offshore wind energy using spaceborne synthetic aperture radar (sar). *Remote Sensing, 14*(7), 1688. https://doi.org/10.3390/rs14071688

Donlon, C. J., Martin, M., Stark, J., Roberts-Jones, J., Fiedler, E., & Wimmer, W. (2012). The operational sea surface temperature and sea ice analysis (ostia) system. [Advanced Along Track Scanning Radiometer] [AATSR]. *Remote Sensing of Environment, 116*, 140–158. https://doi.org/10.1016/j.rse.2010.10.017

Doosttalab, A., Siguenza-Alvaro, D., Pulletikurthi, V., Jin, Y., Bocanegra Evans, H., Chamorro, L. P., & Castillo, L. (2020). Interaction of low-level jets with wind turbines: On the basic mechanisms for enhanced performance. *Journal of Renewable and Sustainable Energy, 12*(5), 053301. https://doi.org/10.1063/5.0017230

Dörenkämper, M., Optis, M., Monahan, A., & Steinfeld, G. (2015). On the offshore advection of boundary-layer structures and the influence on offshore wind conditions. *Boundary-Layer Meteorology, 155*(3), 459–482. https://doi.org/10.1007/s10546-015-0008-x

Dörenkämper, M., Olsen, B. T., Witha, B., Hahmann, A. N., Davis, N. N., Barcons, J., … Mann, J. (2020). The making of the new european wind atlas – part 2: Production and evaluation. *Geoscientific Model Development, 13*(10), 5079–5102. https://doi.org/10.5194/gmd-13-5079-2020

Doyle, J. D., & Warner, T. T. (1993). A three-dimensional numerical investigation of a carolina coastal low-level jet during gale iop 2. *Monthly Weather Review, 121*(4), 1030–1047. https://doi.org/10.1175/1520-0493(1993)121<1030:ATDNIO>2.0.CO;2

Emeis, S. (2014). Wind speed and shear associated with low-level jets over northern germany. *Meteorologische Zeitschrift, 23*(3), 295–304. https://doi.org/10.1127/0941-2948/2014/0551

Gadde, S., & Stevens, R. (2021). Effect of low-level jet height on wind farm performance. *Journal of Renewable and Sustainable Energy, 13*(1), 013305. https://doi.org/10.1063/5.0026232

Gottschall, J., & Dörenkämper, M. (2021). Understanding and mitigating the impact of data gaps on offshore wind resource estimates. *Wind Energy Science, 6*(2), 505–520. https://doi.org/10.5194/wes-6-505-2021

Gross, G. (2012). Numerical simulation of future low-level jet characteristics. *Meteorologische Zeitschrift, 21*(3), 305–311. https://doi.org/10.1127/0941-2948/2012/0279

Gutierrez, W., Araya, G., Kiliyanpilakkil, P., Ruiz-Columbie, A., Tutkun, M., & Castillo, L. (2016). Structural impact assessment of low level jets over wind turbines. *Journal of Renewable and Sustainable Energy, 8*(2), 023308. https://doi.org/10.1063/1.4945359

Hahmann, A. N., Sīle, T., Witha, B., Davis, N. N., Dörenkämper, M., Ezber, Y., … Söderberg, S. (2020). The making of the new european wind atlas – part 1: Model sensitivity. *Geoscientific Model Development, 13*(10), 5053–5078. https://doi.org/10.5194/gmd-13-5053-2020

Hallgren, C., Arnqvist, J., Ivanell, S., Körnich, H., Vakkari, V., & Sahlee, E. (2020). Looking for an offshore low-level jet champion among recent reanalyses: A tight race over the baltic sea. *Energies, 13*(14), 3670. https://doi.org/10.3390/en13143670

Hallgren, C., Aird, J. A., Ivanell, S., Körnich, H., Barthelmie, R. J., Pryor, S. C., & Sahlée, E. (2023). Brief communication: On the definition of the low-level jet. *Wind Energy Science, 8*(11), 1651–1658. https://doi.org/10.5194/wes-8-1651-2023

Heinemann, G., & Zentek, R. (2021). A model-based climatology of low-level jets in the weddell sea region of the antarctic. *Atmosphere, 12*(12), 1635. https://doi.org/10.3390/atmos12121635

Hersbach, H., Bell, B., Berrisford, P., Hirahara, S., Horányi, A., Muñoz-Sabater, J., … Thépaut, J.-N. (2020). The era5 global reanalysis. *Quarterly Journal of the Royal Meteorological Society, 146*(730), 1999–2049. https://doi.org/10.1002/qj.3803

IEC (2022). Wind energy generation systems – part 12–1: Power performance measurements of electricity producing wind turbines, ed. 3.0. Norm.

Kalverla, P. C., Duncan, J. B., Jr., Steeneveld, G. J., & Holtslag, A. A. M. (2019). Low-level jets over the north sea based on era5 and observations: Together they do better. *Wind Energy Science, 4*(2), 193–209. https://doi.org/10.5194/wes-4-193-2019

Kalverla, P. C., Holtslag, A. A. M., Ronda, R. J., & Steeneveld, G. J. (2020). Quality of wind characteristics in recent wind atlases over the north sea. *Quarterly Journal of the Royal Meteorological Society, 146*(728), 1498–1515. https://doi.org/10.1002/qj.3748

Kilpeläinen, T., Vihma, T., Manninen, M., Sjöblom, A., Jakobson, E., Palo, T., & Maturilli, M. (2012). Modelling the vertical structure of the atmospheric boundary layer over arctic fjords in svalbard. *Quarterly Journal of the Royal Meteorological Society, 138*(668), 1867–1883. https://doi.org/10.1002/qj.1914

Lampert, A., Bernalte Jimenez, B., Gross, G., Wulff, D., & Kenull, T. (2015). One year observations of the wind distribution and low-level jet occurrence at Braunschweig, north german plain. *Wind Energy.* https://doi.org/10.1002/we.1951

Larsén, X. G., & Fischereit, J. (2021). A case study of wind farm effects using two wake parameterizations in the weather research and forecasting (wrf) model (v3.7.1) in the presence of low-level jets. *Geoscientific Model Development, 14*(6), 3141–3158. https://doi.org/10.5194/gmd-14-3141-2021

Li, H., Claremar, B., Wu, L., Hallgren, C., Körnich, H., Ivanell, S., & Sahlée, E. (2021). A sensitivity study of the wrf model in offshore wind modeling over the baltic sea. *Geoscience Frontiers, 12*(6), 101229. https://doi.org/10.1016/j.gsf.2021.101229

Luiz, E., & Fiedler, S. (2024). Global climatology of low-level-jets: Occurrence, characteristics, and meteorological drivers. *Journal of Geophysical Research, 129*, e2023JD040262. https://doi.org/10.1029/2023JD040262.

López-García, V., Neely, R., III, Dahlke, S., & Brooks, I. (2022). Low-level jets over the arctic ocean during mosaic. *Elementa, 10*(1), 117–144. https://doi.org/10.1525/elementa.2022.00063

Manzano-Agugliaro, F., Sanchez-Calero, M., Alcayde, A., San-Antonio-Gomez, C., Pereo-Moreno, A. J., & Salmeron-Manzano, E. (2020). Wind turbine offshore foundations and connections to grid. *Inventions, 5*(1), 8. https://doi.org/10.3390/inventions5010008

Marke, T., Crewell, S., Schemann, V., Schween, J., & Tuononen, M. (2018). Long-term observations and high-resolution modeling of midlatitude nocturnal boundary layer processes connected to low-level jets. *Journal of Applied Meteorology and Climatology, 57*(5), 1155–1170. https://doi.org/10.1175/JAMC-D-17-0341.1

Perkovic, L., Silva, P., Ban, M., Kranjcevic, N., & Duic, N. (2013). Harvesting high altitude wind energy for power production: The concept based on magnus' effect. *Applied Energy, 101*, 151–160. https://doi.org/10.1016/j.apenergy.2012.06.061

Platis, A., Bange, J., Bärfuss, K., Cañadillas, B., Hundhausen, M., Djath, B., … Emeis, S. (2020). Long-range modifications of the wind field by offshore wind parks results of the project wipaff. *Meteorologische Zeitschrift, 29*(5), 1–22. https://doi.org/10.1127/metz/2020/1023

Pryor, S. C., Shepherd, T. J., Barthelmie, R. J., Hahmann, A. N., & Volker, P. (2019). Wind farm wakes simulated using WRF. *Journal of Physics: Conference Series, 1256*(1), 012025. https://doi.org/10.1088/1742-6596/1256/1/012025

Ranjha, R., Svensson, G., Tjernström, M., & Semedo, A. (2013). Global distribution and seasonal variability of coastal low-level jets derived from era-interim reanalysis. *Tellus. Series A, Dynamic Meterology and Oceanography, 65*(1), 20412. https://doi.org/10.3402/tellusa.v65i0.20412

Rausch, T., Cañadillas, B., Hampel, O., Simsek, T., Tayfun, Y. B., Neumann, T., … Lampert, A. (2022). Wind lidar and radiosonde measurements of low-level jets in coastal areas of the german bight. *Atmosphere, 13*(5), 839. https://doi.org/10.3390/atmos13050839

Rubio, H., Kühn, M., & Gottschall, J. (2022). Evaluation of low-level jets in the southern baltic sea: A comparison between ship-based lidar observational data and numerical models. *Wind Energy Science, 7*(6), 2433–2455. https://doi.org/10.5194/wes-7-2433-2022

Sandu, I., Beljaars, A., Bechtold, P., Mauritsen, T., & Balsamo, G. (2013). Why is it so difficult to represent stably stratified conditions in numerical weather prediction (nwp) models? *Journal of Advances in Modeling Earth Systems, 5*(2), 117–133. https://doi.org/10.1002/jame.20013

Schulz-Stellenfleth, J., Emeis, S., Dörenkämper, M., Bange, J., Cañadillas, B., Neumann, T., … Lampert, A. (2022). Coastal impacts on offshore wind farms? a review focussing on the german bight area. *Meteorologische Zeitschrift, 31*(4), 289–315. https://doi.org/10.1127/metz/2022/1109

Siedersleben, S. K., Platis, A., Lundquist, J. K., Lampert, A., Bärfuss, K., Cañadillas, B., … Emeis, S. (2018). Evaluation of a wind farm parametrization for mesoscale atmospheric flow models with aircraft measurements. –. *Meteorologische Zeitschrift, 27*(5), 401–415. https://doi.org/10.1127/metz/2018/0900

Skamarock, W., Klemp, J., Dudhia, J. Gill, D., Liu, Z., Berner, J. Wang, W., Power, J., Duda, M., Barker, D., Huang, X. Y. (2019). A description of the advanced research WRF version 3. Technical Report, 162 pages NCAR/TN-556+STR, NCAR – National Center for Atmospheric Research, Boulder, Colorado, USA. https://doi.org/10.5065/1dfh-6p97

Smedman, A. S., Ulf, H., & Hans, B. (1996). Low level jets – a decisive factor for off-shore wind energy siting in the baltic sea. *Wind Engineering, 20*, 137–147.

Stull, R. B. (1988). *An Introduction to Boundary Layer Meteorology*. Dordrecht: Kluwer Academic Publishers. https://doi.org/10.1007/978-94-009-3027-8

Surridge, A. D. (1986). The evolution of the nocturnal temperature inversion. *Boundary-Layer Meteorology, 36*(3), 295–305. https://doi.org/10.1007/BF00118666

Svensson, N., Bergström, H., Sahlee, E., & Rutgersson, A. (2016). Stable atmospheric conditions over the baltic sea: Model evaluation and climatology. *Boreal Environment Research, 21*, 387–404.

Tjernström, M., Leck, C., Persson, P., Jensen, M., Oncley, S., & Targino, A. (2004). The summertime arctic atmosphere: Meteorological measurements during the arctic ocean experiment 2001. *Bulletin of the American Meteorological Society, 85*(9), ES14–ES18. https://doi.org/10.1175/BAMS-85-9-Tjernstrom

Tuononen, M., Sinclair, V., & Vihma, T. (2015). A climatology of low-level jets in the mid-latitudes and polar regions of the northern hemisphere. *Atmospheric Science Letters, 16*(4), 492–499. https://doi.org/10.1002/asl.587

Veers, P., Dykes, K., Lantz, E., Barth, S., Bottasso, C. L., Carlson, O., … Wiser, R. (2019). Grand challenges in the science of wind energy. *Science, 366*(6464), eaau2027. https://doi.org/10.1126/science.aau2027

Wagner, D., Steinfeld, G., Witha, B., Wurps, H., & Reuder, J. (2019). Low level jets over the southern north sea. *Meteorologische Zeitschrift, 28*(5), 389–415. https://doi.org/10.1127/metz/2019/0948

Wagner, R., Antoniou, I., Pedersen, S., Courtney, M., & Jorgensen, H. (2009). The influence of the wind speed profile on wind tur-

bine performance measurements. *Wind Energy, 12*(4), 348–362. https://doi.org/10.1002/we.297

Wagner, R., Courtney, M., Gottschall, J., & Lindelow, P. (2011). Accounting for the speed shear in wind turbine power performance measurement. *Wind Energy, 14*(8), 993–1004. https://doi.org/10.1002/we.509

Wagner, R., Cañadillas, B., Clifton, A., Feeney, S., Nygaard, N., Poodt, M., … Wagenaar, J. (2014). Rotor equivalent wind speed for power curve measurement – comparative exercise for iea wind annex 32. *Journal of Physics: Conference Series, 524*, 012108. https://doi.org/10.1088/1742-6596/524/1/012108

Weide Luiz, E., & Fiedler, S. (2022). Spatiotemporal observations of nocturnal low-level jets and impacts on wind power production. *Wind Energy Science, 7*(4), 1575–1591. https://doi.org/10.5194/wes-7-1575-2022

WRF Users Page (2020). WRF model physics options and references. last accessed: 13.07.2020.

Ziemann, A., Galvez Arboleda, A., & Lampert, A. (2020). Comparison of wind lidar data and numerical simulations of the low-level jet at a grassland site. *Energies, 13*(23), 6264. https://doi.org/10.3390/en13236264

Manuscript received: May 15, 2023
Revisions requested: January 7, 2024
Revised version received: May 8, 2024
Manuscript accepted: September 30, 2024